Available online at www.sciencedirect.com
SCIENCE DIRECT
Coastal Engineering 53 (2006) 81 – 92
Coastal Engineering
An International Journal for Coastal, Harbour and Offshore Engineers
www.elsevier.com/locate/coastaleng

Incipient motion of coarse particles under regular shoaling waves

Emanuele Terrile [a,b], Ad J.H.M. Reniers [a], Marcel J.F. Stive [a,*], Maarten Tromp [a], Henk Jan Verhagen [a]

[a] *Delft University of Technology, The Netherlands*
[b] *University of Genoa, Italy*

Received 20 December 2004; received in revised form 18 March 2005; accepted 24 August 2005
Available online 28 November 2005

Abstract

Incipient motion of coarse particles under regular shoaling waves is examined. Experiments are performed to investigate the effects of bed fluid acceleration on coarse particle stability. By varying wave height, wave period and water depth, combinations of similar peak orbital velocities and weak to strong intra-wave accelerations were created. The particles used in these experiments have two different sizes both of a centimeter order-of-magnitude. The data confirm that acceleration is important for the initiation of motion, since combinations of similar orbital velocity and varying acceleration magnitude resulted in no motion, some motion and motion as acceleration increased. Qualitatively we found that initiation of motion occurs at or is very close to the maximum shear stress due to the combined effects of drag/lift and acceleration as introduced by Nielsen and Callaghan [Nielsen, P. and Callaghan, D.P. (2003), Shear stress and sediment transport calculations for swash zone modelling. Coastal Engineering, 47, pp. 347–354]. However, quantitatively their formulation does not lead to convincing discrimination between motion and no-motion. We expect this to be due to the assumption that the coefficients for drag/lift and acceleration in their formulation are taken equal and constant. From literature and from plotting our data against the Keulegan–Carpenter number we expect that these coefficients strongly vary due to flow separation effects.

To arrive at a more convincing discrimination between motion and no-motion we introduce a new fluid acceleration descriptor for nonlinear shoaling waves. The combination of this descriptor with a Reynolds number Re_g more clearly delineates the regions with particle motion and without particle motion and has the potential to serve as a descriptor of the incipient motion of coarse particles under nonlinear and skewed, regular waves.

Keywords: Incipient particle motion; Skewed waves; Wave acceleration; KC-number

1. Introduction

Coastal sediment transport researchers have been aware of the importance of fluid accelerations or the associated horizontal pressure gradients for a long time. Bagnold (1963) already recognised the potential importance of wave-induced accelerations in general. Madsen (1974) showed that horizontal pressure gradients associated with steep fronts of waves or bores might induce bulk instability and hence vastly enhanced shoreward sediment transport. Nielsen (1979) discussed the likely Keulegan–Carpenter number effects associated with accelerations in wave sediment transport. Hallermeier (1980) experimentally investigated initiation of motion by regular, symmetric waves for relatively coarse sand and showed that a Shields-like parameter could describe the discrimination between motion and no-motion. An interesting experiment was done by King (1991) measuring different net sediment transport rates for forward facing and backward facing saw-tooth half-waves. The importance of surf zone waves often having saw-tooth asymmetry was discussed by Nielsen (1992), who points out that this leads to acceleration asymmetry and to thinner boundary layers (~greater shear stresses) associated with those peak velocities, which follow the briefest acceleration process. Sleath (1994) defined a quasi-steady regime and a pressure gradient regime for coastal sediment transport separated by the value of an acceleration

* Corresponding author.
E-mail addresses: Terrile@diam.unige.it (E. Terrile), A.J.H.M.Reniers@citg.tudelft.nl (A.J.H.M. Reniers), M.J.F.Stive@citg.tudelft.nl (M.J.F. Stive), Maarten@terwa.nl (M. Tromp), H.J.Verhagen@citg.tudelft.nl (H.J. Verhagen).

0378-3839/$ - see front matter © 2005 Elsevier B.V. All rights reserved.
doi:10.1016/j.coastaleng.2005.08.004

parameter, and in several subsequent works, e.g. Zala-Flores and Sleath (1998) and Sleath (1999) acceleration effects in wave-induced sediment transport were quantified in terms of this parameter. The sheetflow data of Ribberink et al. (2000) showed that real waves in a flume, as opposed to Stokes-wave-like velocities in U-tubes generated at least two times more sediment transport for the same orbital velocity magnitude, a difference which could be due to either saw-tooth asymmetry or boundary layer streaming being present in the flume waves but not in the U-tube experiments. The discussion of Nielsen and Callaghan (2003) subsequently provided quantitative estimates of the relative importance of streaming versus acceleration asymmetry. Drake and Calantoni (2001) made a quantitative process-based model to incorporate the effect of pressure gradients on particle motions. Hoefel and Elgar (2003) used their sediment transport skewness formulation to show that flow acceleration may play a role in predicting onshore bar movement under moderate wave conditions. Although the effect of flow acceleration for fine particles is not well established yet, the above findings inspired our research group to undertake a series of experiments to further explore the role of flow acceleration. Since the effect is stronger because pressure (~acceleration) forces scale with the particle diameter cubed while the drag force scales with the particle diameter squared, we decided to undertake experiments for unsteady flow with coarse particles of (O) centimeter diameter. In the region just before wave breaking, near-bed fluid accelerations are found to be strong enough to move the coarse sediment. While the relevance for sand transport has yet to be established, the relevance for stability of bed protection and for onshore gravel transport clearly exists.

2. Experimental set-up and method

The experiments were carried out in a wave flume of the Laboratory of Fluid Mechanics of Delft University of Technology. The glass-walled flume has an effective length of 42.00 m, a width of 0.80 m and a height of 1.00 m. On the bottom of the flume a concrete slope was constructed with a gradient of 1:30 (Fig. 1). Regular waves were generated with a wave paddle using second order wave steering and measurements were confined to the shoaling region. Surface elevations were measured with six resistance type wave gauges (Fig. 1). In order to mitigate the influence of re-reflecting waves in the flume, an Active Reflection Compensation system was used (Klopman, 1995). Measurements confirmed that reflection coefficients on the 1 in 30 slope were low, viz. 1.2% on average.

Table 1
Classes of particle motions

Particle motion percentage	Classification
Less than 25%	Never
Between 25% and 75%	Sometimes
More than 75%	Always

Fluid motions were measured with an EMS (Electro Magnetic Flow Sensor) positioned about 5 cm above the bottom at various locations along the slope. Intra-wave variation of the orbital velocities and accelerations were derived by ensemble-averaging over the wave phase (records between 30–50 s were used implying averaging over 10 to 16 waves).

Two types of nearly uniform coarse particles ($D_{90}/D_{10}\cong 1.25$) were applied in the experiments: $D_{50}=8.8$ mm and $D_{50}=11.4$ mm. The specific density of the particles was 2.67 kg/m^3. In the shoaling region 5 strips of coloured particles (different colours per strip) were placed that could move, while outside these strips the particles were fixed to the bottom. For each test performed the number of particles was determined that moved by observing the measuring area at a particular strip, and the associated forcing wave flow properties, viz. the intra-wave near-bed velocity and acceleration variations. The tests were carried out with different wave periods in the range between $T=2$ s and $T=4.4$ s, with different wave heights: 0.125, 0.15, 0.175 and 0.20 m and at two water depths $h=0.60$ and 0.65 m, respectively.

In order to create a statistically significant dataset, a sufficient number of forcing situations are needed to establish the threshold of particle motion, i.e. we need a sufficient number of situations with similar orbital velocity magnitudes in combination with small to large acceleration magnitudes. Some of these combinations did not lead to particle movement while others with similar orbital velocities but larger acceleration did lead to particle movement. To establish a reliable percentage of particle motion, tests with near-equal velocities and accelerations for which particle motion occurred were repeated multiple times (up to 6 or 7 times). In doing so we were able to reduce stochastic effects, for instance, due to insufficient settling time of the bed after placing which can result in a motion-favourable position for a particle. A total of 117 experimental results were

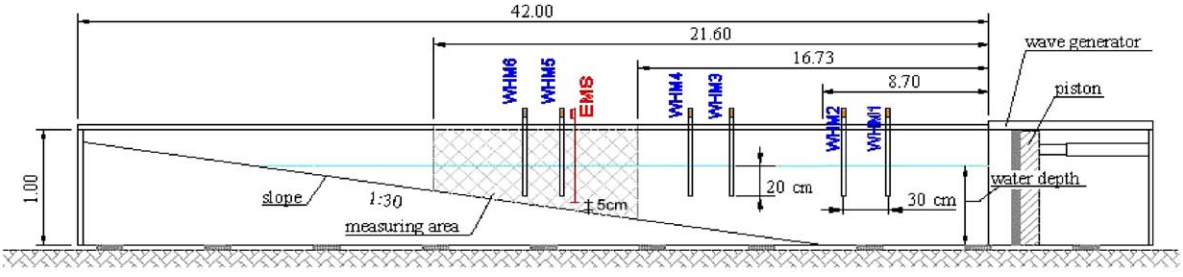

Fig. 1. Flume dimensions and location of measurement instruments along the slope (horizontal dimensions in meters).

established covering a range of orbital velocities and orbital accelerations.

As indicated, the stochastic nature of the particle motion needs consideration; therefore we have categorized the particle motion in classes (Table 1). Threshold of motion is defined as motion of at least 3 coloured particles out of a coloured strip. Motion of particles within the relatively narrow strips is not considered as motion. The percentages refer to the ratio of the times that three stones moved over the total times that particle motion was assessed under near-equal conditions.

Using motion of at least three particles reduces the influence of a motion-favourable orientation of a particle in the bed. A sensitivity analysis, in which the data of the motion of one and four particles were also analysed, showed small differences with the results found for the chosen criterion of motion of three particles (Terrile, 2004).

The above approach results in a dataset which determines no, some, or significant particle movement with associated peak orbital motion and a representative measure of acceleration (see Appendix). This dataset forms the basis of our analysis presented below.

3. Data analysis

As a first step in our data analysis we compare our results with the classical findings of Hallermeier (1980). As far as we are aware this author was the first to undertake experiments for initiation of sediment motion under regular, non-shoaling waves. By analysing his data, Hallermeier showed that the following relation produced a good discrimination between motion and no-motion.

$$\frac{A}{D} = \left(\frac{8(s-1)g}{\omega^2 D}\right)^{0.5} \tag{1}$$

where A is the wave excursion, D the diameter of the spherical grains, s is the relative density (ρ_s/ρ), g the acceleration of gravity, and ω is the angular frequency ($2\pi/T$). If following Nielsen (1992) we define a Shields-like parameter:

$$\theta = \frac{0.5f(A\omega)^2}{(s-1)gD} \tag{2}$$

where f is a wave friction factor. It can be shown that Hallermeier's expression can then be rewritten to yield:

$$\theta = 4f \tag{3}$$

Hence Hallermeier's Eq. (1) is basically a Shields-like parameter, which expresses the ratio of gravity force over drag/lift force. Fig. 2 displays our results versus Hallermeier's empirical relation. Obviously, acceleration effects were present in Hallermeier's experiments, but were not explicitly accounted for. We note three important findings. Firstly, our results indicate motion for much lower values than Hallermeier's expression, which we either contribute to the absence in his expression of increased acceleration effects of our skewed waves or to the fact that our results are in a different diameter regime. Secondly, there appears to be no discrimination between our results for motion and no-motion. This is obviously due to the fact that no discriminative acceleration effects are included in Hallermeier's parameter. Thirdly, an interesting qualitative difference between our results and the empirical fit of Hallermeier is observed. If we interpret our results as "close-to-initiation-of-motion", we observe not a linear, but a nonlinear relation. This implies that the Shields-like parameter is not constant, but a function of the Reynolds number. This will be discussed further on.

As a second step in our data analysis we discuss our visual and video observations. Fig. 3 depicts a typical time evolution of the free stream orbital velocity and the associated accelerations. Initiation of motion was observed to occur consistently in between the moment of maximum acceleration (point B) and the moment of maximum onshore flow velocity (point C). Apparently, the combination in this region of high acceleration

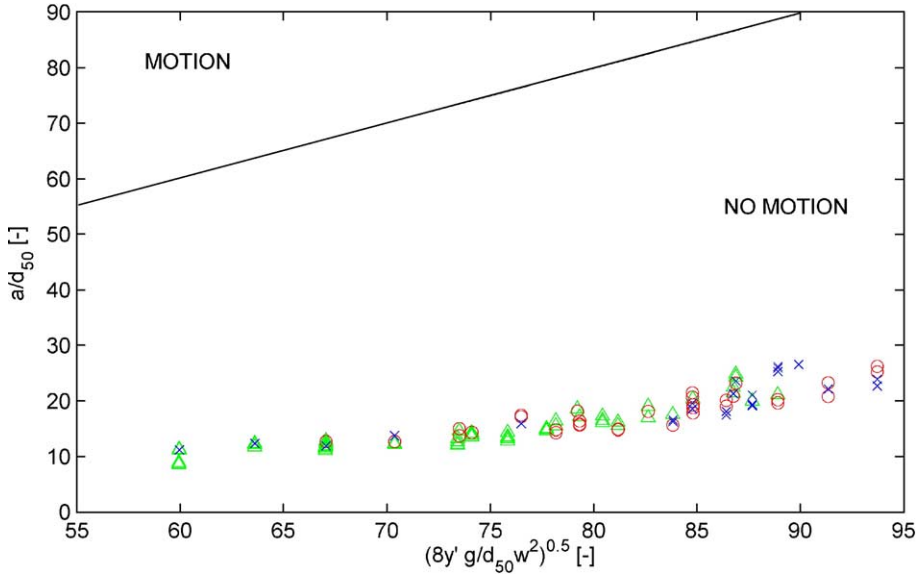

Fig. 2. Comparison of Hallermeier's Eq. (1) with our test data, where the symbols indicate (△) never, (○) sometimes, (×) always motion.

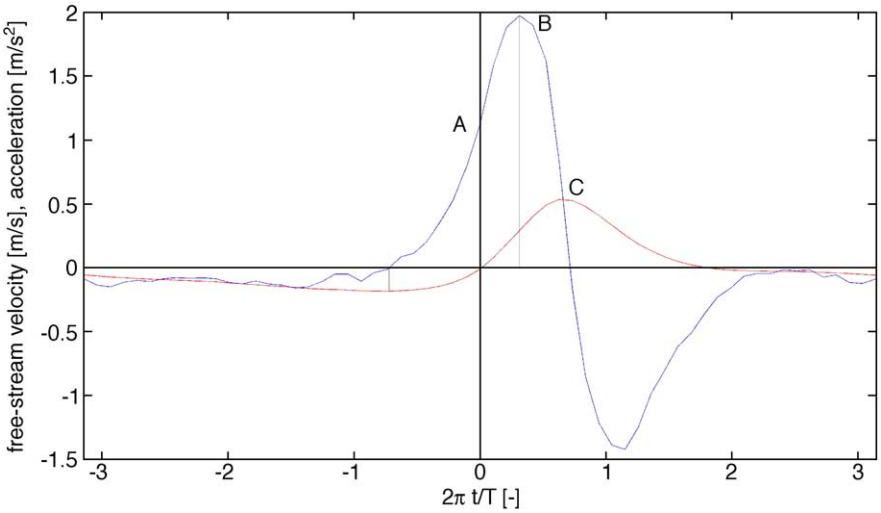

Fig. 3. Typical time series of near-bed velocity (red line) and acceleration (blue line). (For interpretation of the references to colour in this figure legend, the reader is referred to the web version of this article.)

and high free stream velocity creates an optimum condition for sediment particle motion.

The above analysis can be made quantitative by making use of the formulation proposed by Nielsen (1992, 2002) and Nielsen and Callaghan (2003) for the Shields parameter in an unsteady turbulent flow:

$$\theta_a(t) = \frac{\frac{1}{2}f_{2.5}}{(s-1)gD_{50}}\left(u_\infty \cos\varphi_\tau + \frac{1}{\omega_p}\sin\varphi_\tau \frac{du_\infty}{dt}\right)^2 \times sign(u*(t)) \quad (4)$$

where $f_{2.5}$ is the wave friction factor (Jonsson, 1966; Svendsen and Jonsson, 1976) corresponding to a bed roughness of $2.5D_{50}$ (Nielsen, 1992), u_∞ is the free stream velocity, ω_p is the peak angular frequency $(2\pi/T)$ and φ_τ is the phase shift between free stream velocity and bed shear stress at the peak frequency. Note that in contrast to Nielsen (1992) the square of the summed effect instead of a linear summation of shear velocity and acceleration is taken to account for strongly turbulent flow instead of laminar flow. Also note that for both effects the same coefficient ($f_{2.5}$) is used, which will be discussed below.

Eq. (4) expresses both the effect of shear velocity (first term) and of acceleration (second term) on the Shields parameter θ_a. Making use of our measurements and by adopting a value of $1/18\pi$ for φ_τ (which we have quantified from video observations and which is in line with Fredsøe and Deigaard, 1992) we have computed a typical intra-wave variation of the three contributing terms (Fig. 4). The solid line, containing the symbol ○, represents the pure velocity contribution $(u_\infty \cos\varphi_\tau)^2$, the solid line, containing the symbol ×, represents the acceleration contribution $(1/\omega_p \sin\varphi_\tau\ du_\infty/dt)^2$, the solid line, containing the symbol △, represents their cross-product $(u_\infty \cos\varphi_\tau\ 1/\omega_p \sin\varphi_\tau\ du_\infty/dt)$ and the dash dot line the total value of the stability parameter θ_a.

All three contributions are positive and strong for the particular region between point B and the passage of the wave crest. The instant at which the sum of these three terms is

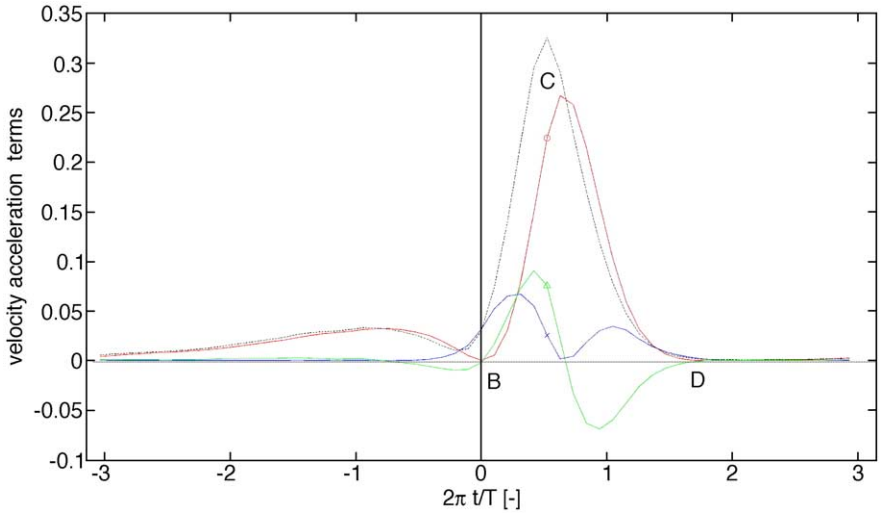

Fig. 4. Velocity and acceleration terms of the stability parameter and the total stability parameter θ_a for a wave with period $T=3$ s and wave height $H=0.15$ m.

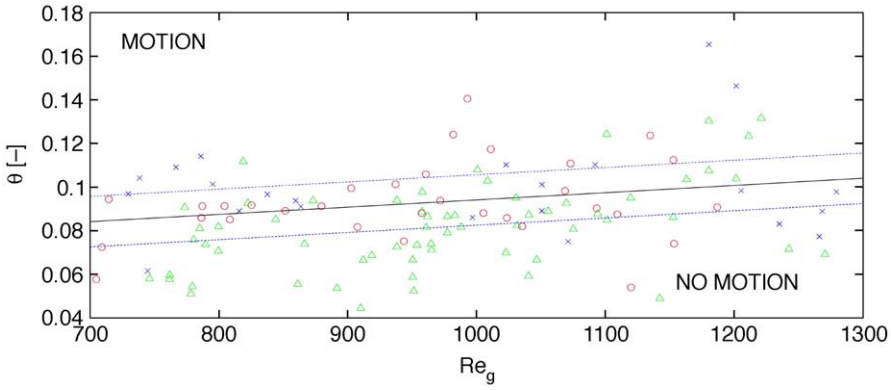

Fig. 5. Shields-like presentation of Nielsen's max shear stress θ versus Re_g based on our test data, where the symbols indicate (△) never, (○) sometimes, (×) always motion. See text for explanation of the definition of the regression line and the bandwidths.

maximum, corresponding to a maximum value of the Shields number, is marked by the three symbols (△), (×) and (○). This corresponds to the region between (point B) and the maximum onshore free stream velocity (point C), and is equal or very close to the instant of motion initiation that we have observed from video.

Qualitatively these results support Nielsen and Callaghan's (2003) formulation as given by Eq. (4), i.e. we observe that the maximum value of their formulation correlates clearly with the instant of motion initiation. Following Shields we therefore introduce a particle Reynolds-like number, since it is clear that the maximum orbital velocity and the stone diameter play a role as well:

$$Re_g = \frac{u_{\mathrm{rms}} D_{50}}{\nu} \tag{5}$$

where ν is the kinematic viscosity of the fluid and $u_{\mathrm{rms}} = \sqrt{Var[u_\infty(t)]}$.

Fig. 5 shows Nielsen and Callaghan's (2003) formulation for our experiments against the particle Reynolds-like number. Here and in the following figures we have determined a regression line based on some motion results, and we have indicated a lower and upper bandwidth with equal intervals in which 63% of some motion results fall. Where the regression line may be used to assess a critical threshold for motion, the lower bandwidth line may be used to assess static stability. The discrimination skill is now determined as the percentage of some motion and motion data above the regression line and above the lower bandwidth line minus the percentage of no-motion data above these lines. In the former case the skill is 28.7% and the latter case 33.4%. As we observe there is not a very convincing discrimination, which is rather surprising because of the qualitative agreement concluded before.

As a next step in our further exploration of the issue we decided to first look for a more convincing discrimination between motion and no-motion by presenting our data as a function of a representative acceleration value, since our dataset contains situations with a similar orbital flow velocity and varying acceleration. From the above findings we concluded that two acceleration values play a crucial role in the process of initiation of motion, viz. a_0 being the value of acceleration at the beginning of the growth of the boundary layer when the velocity is zero and changing to onshore flow (point A in Fig. 3) and $a_{\max}$ being the maximum of the near-bed fluid acceleration (point B in Fig. 3). Obviously $a_{\max}$ should be large, but when a_0 is large as well the waves are either very skewed (saw-tooth like) or highly nonlinear in a horizontal sense (horizontally asymmetric) and in both cases both the shear velocity and the acceleration are large, the combination of which favours motion. Therefore when the product of these values is large we should expect the conditions most conducive for initiation of particle motion due to the

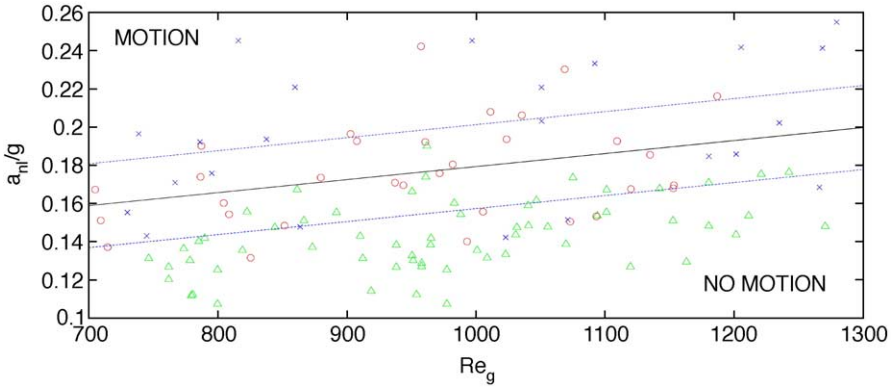

Fig. 6. Shields-like presentation of the acceleration parameter a_{nl}/g versus Re_g based on our test data, where the symbols indicate (△) never, (○) sometimes, (×) always motion. See text for explanation of the definition of the regression line and the bandwidths.

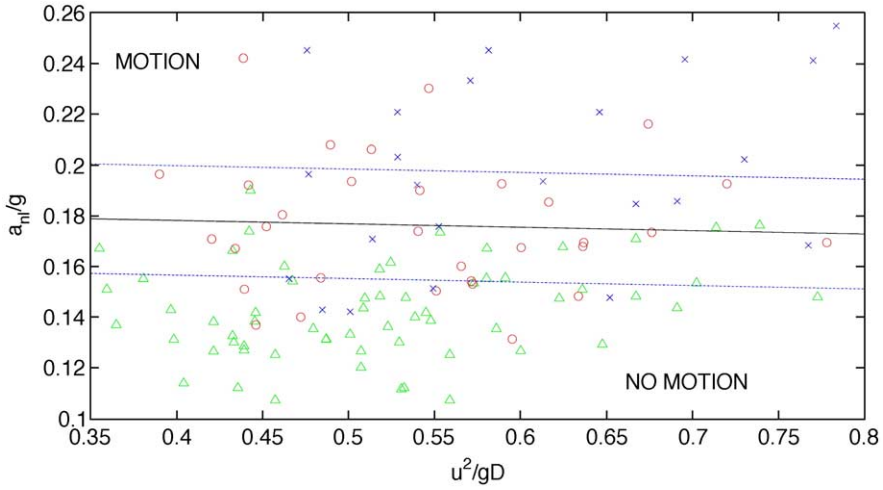

Fig. 7. Threshold of motion as a function of the acceleration parameter a_{nl}/g and the drag/lift parameter u_{rms}^2/gD_{50} based on our test data, where the symbols indicate (△) never, (○) sometimes, (×) always motion. See text for explanation of the definition of the regression line and the bandwidths.

acceleration. We thus introduce a new dimensional acceleration descriptor for nonlinear waves defined as follows:

$$a_{nl} = \sqrt{a_{max} a_0}. \tag{6}$$

The following properties for a_{nl} are noted. Its value always lies between the value of a_0 and a_{max}; in case of skewed waves, the closer it is to a_{max} the skewer or the more horizontally asymmetric the waves are. For waves that are horizontally asymmetric only, a_0 and a_{max} could be either the accelerations at and right after the change to onshore or the accelerations just before and at the change to offshore flow. In both cases the initiation of motion should be similar. For pure sinusoidal waves no difference between a_{max} and a_0 exists, hence a_{max} is a_0, so $a_{nl}=a_0$, denoting minimal acceleration effects (as is expected to be the case for Hallermeier's results).

All our experimental results are collected in Fig. 6 where for each test the measured a_{nl}, made dimensionless by the acceleration of gravity, is plotted versus the particle Reynolds-like number Re_g. Apparently, for a particular value of Re_g we observe a critical value of a_{nl}. When $a_{nl} \geq a_{nl,crit}$ the particles start to move. Now a more convincing division is observed between a region in which there is always movement and one where there is no movement. This is also observed in the discrimination skills, viz. 51.1% for the regression line and 56.0% for the lower bandwidth line.

Note that Re_g increases with D_{50} when u_{rms} is constant. If we expect the acceleration to play a role, initiation of motion

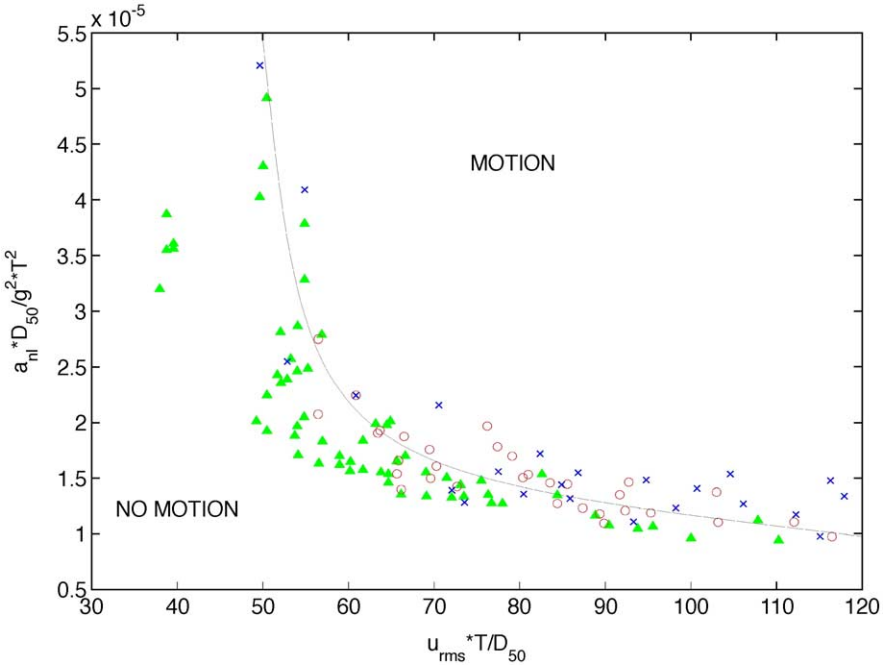

Fig. 8. Threshold of motion as a function of the acceleration parameter $a_{nl}\,D_{50}/g^2T^2$ and the Keulegan–Carpenter number $u_{rms}\,T/D_{50}$ based on our test data, where the symbols indicate (△) never, (○) sometimes, (×) always motion.

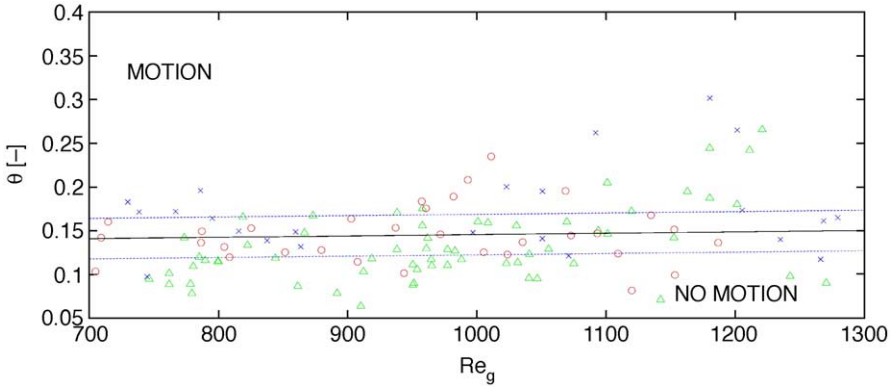

Fig. 9. Shields-like presentation of Nielsen's max shear stress θ (based on $C_d \approx 0.2C_m$) versus Re_g based on our test data, where the symbols indicate (△) never, (○) sometimes, (×) always motion. See text for explanation of the definition of the regression line and the bandwidths.

should occur for larger values of a_{nl}, which is what we observe. On the other hand Re_g also increases with u_{rms} while D_{50} is constant. Apparently, even when the orbital velocity increases, we need an associated increase of acceleration, such that initiation of motion occurs only for larger values of a_{nl}. Initially we found these results difficult to interpret physically.

To extend our analysis we chose to plot (see Fig. 7) a_{nl}/g versus $u_{rms}^2/(gD_{50})$, which represent the two "Morrison-like" theoretical forces (pressure gradient and drag/lift) that cause the motion. The discrimination skills are very reasonable, viz. 44.3% for the regression line and 50.6% for the lower bandwidth line. However, we expected a clear linear decrease of the threshold motion line expressing compensation of the one force by the other, but whereas the drag/lift force varies by a factor of two the acceleration force hardly varies. Both these results (Figs. 6 and 7) can only be explained when the C_d coefficient (the combined drag/lift coefficient) decreases stronger than the C_m coefficient (the acceleration coefficient) as Re_g increases and consequently a higher acceleration effect is required to compensate for the decrease in shear velocity effect. Looking at the results of Keulegan and Carpenter (1958) and Sarpkaya (1976) this can be observed to be the case for a variety of experiments in ranges of the Reynolds-like number similar to our experiments. These conclusions are confirmed by plotting our results against the Keulegan–Carpenter number in Fig. 8, which indicates that apparently our results fall in the region where strong variations are encountered in the degree of flow separation which influences both drag and acceleration. This conclusion makes the use of the same coefficient for the drag/lift and acceleration effect in Eq. (4) (both C_m and C_d are equal to $f_{2.5}$) a questionable assumption.

From analysis of similar data by Tromp (2004) it was suggested that there might be a difference of as much as a factor of 5 between C_m and C_d, viz. $C_d \approx 0.2C_m$. Hence we applied this finding to Eq. (4). The results given in Fig. 9 indicate that indeed a difference in discrimination is found

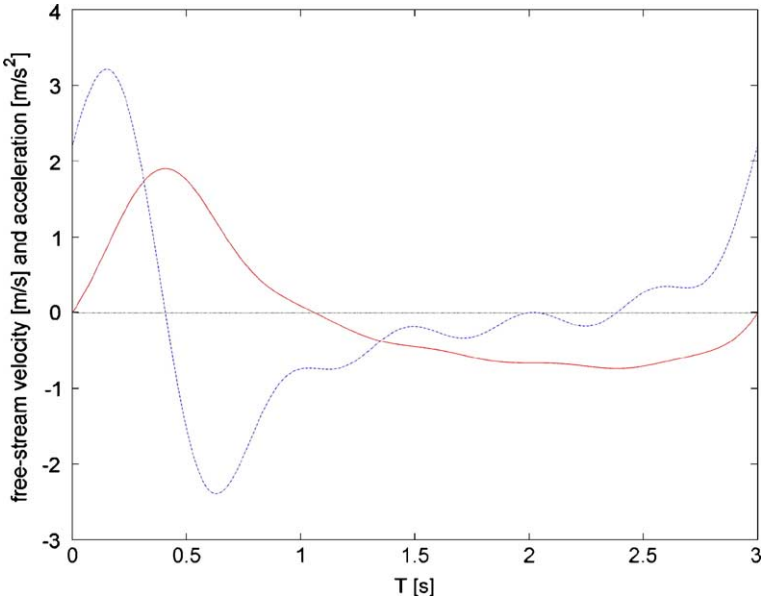

Fig. 10. Time series of near-bed velocity (solid line) and acceleration (dash dot line) for simulated wave shapes with a waveform parameter $\Phi = 0$ and velocity amplitude $c = 0.5$.

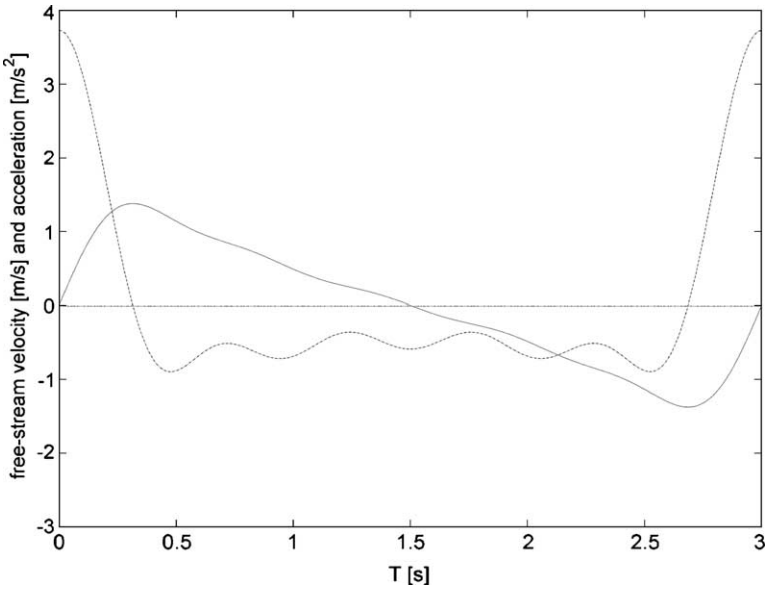

Fig. 11. Time series of near-bed velocity (solid line) and acceleration (dash dot line) for simulated wave shapes with a waveform parameter $\Phi=\pi/2$ and velocity amplitude $c=0.5$.

locally, i.e. local improvement in the lower Re_g region, but overall the discrimination skill is disappointingly similar to the original formulation, viz. 25.7% for the regression line and 31.8% for the lower bandwidth line. Obviously one could make an empirical fit using a variable ratio between C_d and C_m, but we consider this not justified on the basis of this limited dataset.

4. Discussion

In this discussion we address the question whether the new acceleration descriptor a_{nl} has advantages compared to the acceleration descriptor a_{spike} introduced by Drake and Calantoni (2001). To quantify particle flux due to waves that are horizontally asymmetric and skewed they introduced the following formulation:

$$\langle q\rangle = \begin{cases} k\langle u^3\rangle + K_a\left(a_{spike}-a_{crit}\right) & a_{spike}\geq a_{crit} \\ k\langle u^3\rangle & a_{spike}<a_{crit} \end{cases} \quad (7)$$

where k and K_a are empirical parameters, a_{crit} is the critical value of a_{spike} that must be exceeded before acceleration increases transport and $<u^3>$ the average of the cubic of the velocity. Due to the definition of a_{spike} ($=<a^3>/<a^2>$)

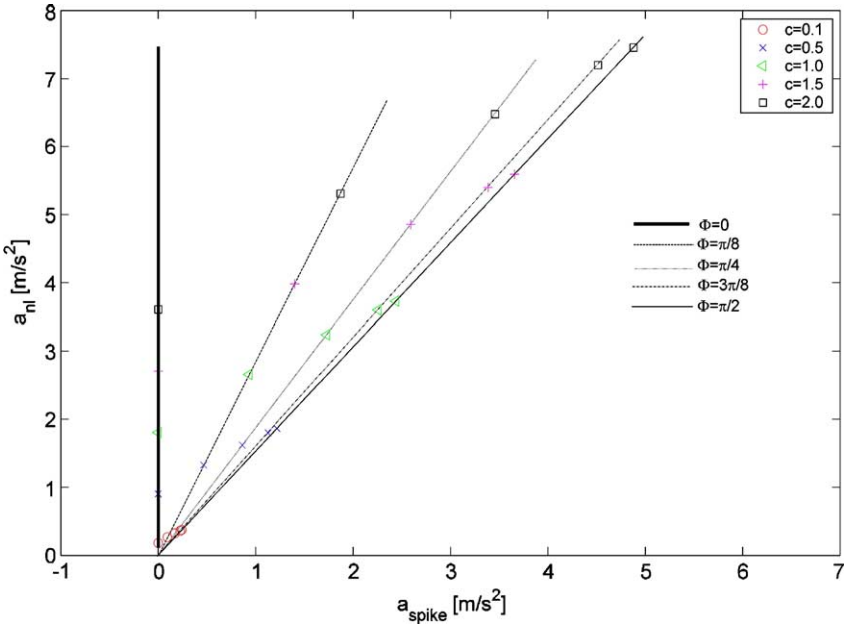

Fig. 12. Relation between a_{nl} and a_{spike} from simulated wave shapes having waveform parameters $\Phi=0$, $\pi/8$, $\pi/4$, $3\pi/8$ and $\pi/2$, $T=6$ s and different velocity amplitudes $c=0.1$, 0.5, 1.0, 1.5 and 2.0 m/s. The value of the waveform parameters increases from 0 to $\pi/2$ from left to right.

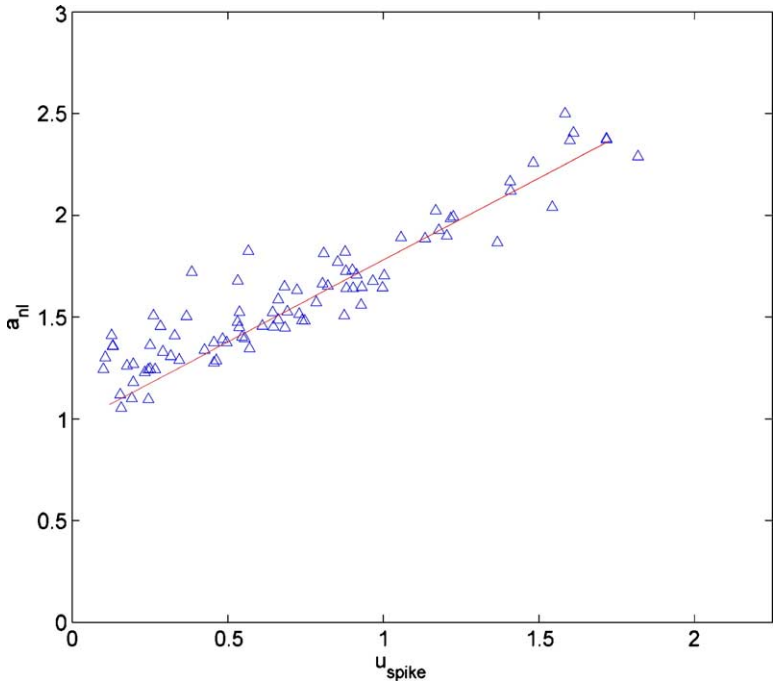

Fig. 13. Relation between a_{nl} and a_{spike} for our experiments.

acceleration effects are absent for waves, which are horizontally asymmetric only. The effect of such waves is included in the average of the cubic of the velocity. In saw-tooth waves the latter effect is absent and a_{spike} represents the effect of acceleration in such waves.

To discuss these properties and those of a_{nl} we explore the relation between a_{nl} and a_{spike}. We therefore simulated a range of different theoretical waveforms and compare the two descriptors. The time-varying velocity used in our simulations is:

$$u(t) = c\sum_{m=0}^{4}\frac{1}{2^m}\cos\left([m+1]\omega_p t + m\Phi\right) \quad (8)$$

where Φ is the waveform parameter defined by Elgar and Guza (1985) and c is a measure of the velocity amplitude.

In our wave experiments the velocity amplitudes have an approximate value of $c=0.5$, while the waveform parameter varies approximately between $\Phi=0$ and $\pi/2$. Figs. 10 and 11 illustrate these two end ranges for the waveform, i.e. solely horizontally asymmetric waves, or $\Phi=0$, and solely skewed waves, or $\Phi=\pi/2$. As stated, in the former case with $\Phi=0$, a_{spike} should be zero by definition in contrast to a_{nl}. In the latter case with $\Phi=\pi/2$, we expect the two descriptors to behave similarly and assume their maximum values.

To quantitatively confirm this behaviour of a_{nl} and a_{spike} we simulated five different waveform parameters, i.e. $\Phi=0$, $\pi/8$, $\pi/4$, $3\pi/8$ and $\pi/2$, and five different values of the velocity amplitude $c=0.1$, 0.5, 1.0, 1.5 and 2.0 m/s. Fig. 12 shows the behaviour of a_{nl} and a_{spike} for the five different waveform parameters and the five velocity amplitudes. It confirms that for $\Phi=0$ a_{spike} remains zero and a_{nl} (similar to and thus potentially a substitute for $<u^3>$) increases due to increasing horizontal asymmetry, while for $\Phi=\pi/2$ a linear proportionality between a_{nl} and a_{spike} is found both with maximum values, confirming the above statements. For mixed waveforms between $\Phi=0$ and $\Phi=\pi/2$ also a linear proportionality occurs because of the mix between horizontal asymmetry and skewness, where the latter dictates the behaviour of a_{spike}. Finally we note that all our experimental results are closely in the range of $c=0.5$ and with the waveform parameter varying between $\Phi=0$ and $\pi/2$. Hence, the results should approximately follow the relation indicated by the crosses ($c=0.5$) in Fig. 12. Fig. 13 confirms this where the variability around the regression line is due to the slight nonlinearity between a_{nl} and a_{spike} and due to the variation of the velocity amplitudes around $c=0.5$.

In conclusion we note that a_{nl} includes both the effect of skewness and horizontal asymmetry. This simultaneous inclusion of skewness and horizontal asymmetry in one acceleration descriptor is attractive in the formulation of future bed load transport formulations.

5. Conclusion

Based on experiments with regular shoaling waves the effects of bed fluid acceleration on coarse particle stability were investigated for two different sizes both of a centimeter order-of-magnitude. By varying wave height, wave period and water depth combinations of similar peak orbital velocities and weak to strong intra-wave accelerations were created. The data confirmed that the acceleration plays a role for the initiation of motion, since combinations of similar orbital velocity and varying acceleration magnitude resulted in no motion, some motion and motion as acceleration increased.

Qualitatively we found that initiation of motion occurs at or is very close to the maximum shear stress due to the combined effects of drag/lift and acceleration as introduced by Nielsen and Callaghan (2003). However, quantitatively their formulation does not lead to convincing discrimination between motion and no motion. We expect this to be due to the assumption that the coefficients for drag/lift and acceleration in their formulation are taken equal. From literature and from plotting our data against the Keulegan–Carpenter number we expect that the coefficients strongly vary caused by flow separation effects.

To arrive at a more convincing discrimination between motion and no-motion we introduced a new fluid acceleration descriptor for nonlinear shoaling waves. The combination of this descriptor with a Reynolds number Re_g clearly delineates the regions with particle motion and without particle motion and has the potential to serve as a descriptor of the incipient motion of coarse particles under nonlinear regular waves. The interesting property of the descriptor is that it simultaneously includes skewness and horizontal asymmetry, which is attractive in the formulation of future bed load transport formulations.

Acknowledgements

The experiments were conducted in a wave flume of the Hydraulics Laboratory of the Faculty of Civil Engineering and Geosciences of Delft University of Technology. Maarten Tromp conducted a first set of experiments as part of his MSc Thesis work, which laid the basis for the experiments conducted by Emanuele Terrile as part of his MSc thesis work (supported by the MSc EU Erasmus programme) reported here. The manuscript improved considerably as a result of a review by an unknown reviewer, but especially by the critical and constructive review by Peter Nielsen. Technical assistance in conducting these experiments by Henry Fontijn is greatly appreciated. The Dutch National Science Foundation (NWO) under contract number DCB5856 funded A.J.H.M.R.

Appendix A

In the following Table A1, we tabulate the results of the 117 experiments: the wave code number, the Reynolds-like number Re_g, the Reynolds-like number Re (using u_{max}), a_{nl} made dimensionless by the acceleration of gravity, the shear stress from Nielsen and Callaghan's θ by using $C_d=0.2\ C_m$, the shear stress from Nielsen and Callaghan's θ by using $C_d=C_m$ and the classes of movement (N: never, S: sometimes and A: always).

Table A1
Data results

Wave code	Re_g [−]	Re [−]	a_{nl}/g [−]	θ [−] Nielsen's eq. with $C_d=0.2\ C_m$	θ [−] Nielsen's eq. with $C_d=C_m$	Movement class
W 1	919	1712	0.114	0.117	0.068	N
W 2	938	1778	0.127	0.128	0.073	N
W 3	958	1918	0.129	0.156	0.089	N
W 4	958	2002	0.127	0.175	0.097	N
W 5	938	2011	0.138	0.171	0.094	N
W 6	1221	2543	0.175	0.262	0.135	N
W 7	1181	2526	0.148	0.198	0.121	N
W 8	781	1681	0.112	0.109	0.076	N
W 9	954	2055	0.112	0.105	0.073	N
W 10	800	1742	0.107	0.114	0.082	N
W 11	977	2130	0.017	0.110	0.079	N
W 12	977	2191	0.125	0.128	0.087	N
W 13	1009	2385	0.131	0.159	0.103	N
W 14	819	2009	0.135	0.166	0.112	N
W 15	1001	2455	0.135	0.160	0.108	N
W 16	774	2002	0.136	0.142	0.091	N
W 17	951	2336	0.130	0.093	0.063	N
W 18	1040	2552	0.159	0.103	0.071	N
W 19	910	2389	0.143	0.069	0.055	N
W 20	965	2429	0.142	0.063	0.050	N
W 21	1041	2570	0.148	0.128	0.092	N
W 22	1094	2878	0.154	0.157	0.093	N
W 23	1101	2970	0.167	0.153	0.090	N
W 24	1153	3062	0.151	0.143	0.091	N
W 25	912	2350	0.131	0.109	0.076	N
W 26	1032	2627	0.147	0.122	0.090	N
W 27	873	2341	0.137	0.120	0.073	N
W 28	1120	2394	0.127	0.170	0.095	N
W 29	1163	2468	0.129	0.194	0.107	N

Table A1 (*continued*)

Wave code	Re_g [−]	Re [−]	a_{nl}/g [−]	θ [−] Nielsen's eq. with C_d=0.2 C_m	θ [−] Nielsen's eq. with C_d=C_m	Movement class
W 30	1023	2310	0.133	0.116	0.073	N
W 31	951	2464	0.166	0.112	0.070	N
W 32	779	1782	0.112	0.078	0.054	N
W 33	962	1832	0.120	0.088	0.058	N
W 34	1056	2640	0.148	0.135	0.093	N
W 35	844	2149	0.147	0.123	0.090	N
W 36	1070	2556	0.139	0.145	0.083	N
W 37	951	2006	0.133	0.073	0.051	N
W 38	965	2226	0.138	0.100	0.063	N
W 39	1101	2675	0.155	0.183	0.113	N
W 40	762	1912	0.127	0.101	0.059	N
W 41	1181	2763	0.171	0.251	0.131	N
W 42	778	1912	0.130	0.084	0.049	N
W 43	1202	2332	0.144	0.177	0.106	N
W 44	1211	2416	0.154	0.227	0.122	N
W 45	823	2120	0.156	0.129	0.096	N
W 46	867	2367	0.151	0.153	0.081	N
W 47	1271	3256	0.148	0.094	0.076	N
W 48	988	2605	0.154	0.113	0.086	N
W 49	983	2508	0.160	0.124	0.088	N
W 50	800	1793	0.125	0.115	0.071	N
W 51	1243	3282	0.176	0.101	0.080	N
W 52	746	1922	0.131	0.096	0.064	N
W 53	1143	2864	0.168	0.077	0.060	N
W 54	1047	2715	0.162	0.099	0.076	N
W 55	790	1987	0.142	0.067	0.050	N
W 56	1075	2754	0.173	0.110	0.083	N
W 57	962	2543	0.190	0.142	0.091	N
W 58	1031	2543	0.144	0.154	0.097	N
W 59	861	2341	0.167	0.085	0.065	N
W 60	785	2063	0.140	0.120	0.081	N
W 61	892	2407	0.155	0.084	0.065	N
W 62	961	2512	0.174	0.134	0.086	N
W 63	1024	2658	0.194	0.116	0.085	S
W 64	1153	2570	0.169	0.107	0.081	S
W 65	825	1951	0.131	0.153	0.092	S
W 66	709	1937	0.151	0.155	0.077	S
W 67	809	2131	0.154	0.115	0.087	S
W 68	957	2372	0.242	0.189	0.093	S
W 69	1005	2592	0.156	0.123	0.091	S
W 70	972	2552	0.176	0.153	0.098	S
W 71	1153	2820	0.168	0.188	0.125	S
W 72	982	2583	0.180	0.236	0.145	S
W 73	1073	2640	0.150	0.171	0.121	S
W 74	1135	2983	0.185	0.187	0.134	S
W 75	993	2587	0.140	0.253	0.155	S
W 76	804	2052	0.160	0.130	0.092	S
W 77	903	2442	0.196	0.164	0.102	S
W 78	1187	3128	0.216	0.169	0.119	S
W 79	714	1915	0.137	0.208	0.127	S
W 80	1109	2534	0.193	0.140	0.104	S
W 81	880	2254	0.173	0.137	0.103	S
W 82	1093	2578	0.153	0.153	0.098	S
W 83	1069	2860	0.230	0.214	0.114	S
W 84	705	1915	0.167	0.122	0.074	S
W 85	851	2102	0.148	0.127	0.091	S
W 86	1120	2847	0.167	0.084	0.058	S
W 87	1036	2715	0.206	0.137	0.081	S
W 88	961	2596	0.192	0.174	0.111	S
W 89	944	2102	0.169	0.116	0.087	S
W 90	787	2081	0.190	0.154	0.099	S
W 91	786	2056	0.174	0.145	0.093	S
W 92	908	2074	0.193	0.113	0.086	S

(continued on next page)

Table A1 (*continued*)

Wave code	Re_g [−]	Re [−]	a_{nl}/g [−]	θ [−] Nielsen's eq. with C_d=0.2 C_m	θ [−] Nielsen's eq. with C_d=C_m	Movement class
W 93	937	2499	0.171	0.157	0.106	S
W 94	1011	2640	0.208	0.262	0.136	S
W 95	997	2284	0.245	0.172	0.106	A
W 96	745	1955	0.143	0.113	0.070	A
W 97	1023	2486	0.142	0.238	0.131	A
W 98	1181	2781	0.185	0.325	0.179	A
W 99	739	1998	0.196	0.172	0.107	A
W 100	838	2174	0.194	0.145	0.105	A
W 101	816	1868	0.245	0.160	0.101	A
W 102	860	1966	0.221	0.169	0.108	A
W 103	1206	3318	0.242	0.193	0.110	A
W 104	1051	2402	0.221	0.161	0.102	A
W 105	1071	2583	0.151	0.145	0.091	A
W 106	864	2160	0.148	0.134	0.093	A
W 107	1266	3454	0.168	0.100	0.068	A
W 108	1202	2552	0.186	0.258	0.148	A
W 109	730	1969	0.155	0.291	0.158	A
W 110	1051	2772	0.203	0.288	0.151	A
W 111	767	2045	0.171	0.189	0.120	A
W 112	795	2088	0.176	0.184	0.111	A
W 113	786	2124	0.192	0.208	0.125	A
W 114	1092	2904	0.233	0.294	0.125	A
W 115	1235	3388	0.202	0.159	0.099	A
W 116	1280	3516	0.255	0.188	0.111	A
W 117	1269	3480	0.241	0.179	0.097	A

References

Bagnold, R.A., 1963. Beach and nearshore processes: Part I. Mechanics of marine sedimentation. In: Hill, N.M. (Ed.), The Sea Vo1 3: The Earth Beneath the Sea, pp. 507–553.

Drake, T.G., Calantoni, J., 2001. Discrete particle mode for sheet flow sediment transport in the nearshore. J. Geophys. Res. Oceans 106 (C9), 19.859–19.868.

Elgar, S., Guza, R.T., 1985. Observation of bispectra of shoaling surface gravity waves. J. Fluid Mech. 167, 425–448.

Fredsøe, J., Deigaard, R., 1992. Mechanics of coastal sediment transport. Advanced Series on Ocean Engineering, vol. 2. World Scientific.

Hallermeier, R.J., 1980. Sand motion initiation by water waves; two asymptotes. Proc. ASCE 106 (WW6), 299–318.

Hoefel, F., Elgar, S., 2003. Wave-induced sediment transport and sand bar migration. Science 299, 1885–1887.

Jonsson, I.G., 1966. Wave boundary layers and friction factor. Proc. 10th ICCE Tokyo. ASCE, New York.

Keulegan, G.H., Carpenter, L.H., 1958. Forces on cylinders and plates in an oscillating fluid. J. Res. Natl. Bur. Stand. 60, 5.

King Jr., D.B., 1991. Studies on oscillatory flow bedload sediment transport. PhD thesis, U. C. San Diego (Scripps).

Klopman, G., 1995. Active wave absorption. WL|Delft Hydraulics, Rep. H1222. Delft Hydraulics, The Netherlands.

Madsen, O.S., 1974. Stability of a sand bed under breaking waves. Proc. 14th Int. Conf. Coastal Eng.. ASCE, Copenhagen, pp. 776–794.

Nielsen, P., 1979. Some basic concepts of wave sediment transport. PhD thesis. Techn. Univ. of Denmark, ISVA Series Paper 20, 160 pp.

Nielsen, P., 1992. Coastal bottom boundary layers and sediment transport. Advanced Series on Ocean Engineering, vol. 4. World Scientific.

Nielsen, P., 2002. Shear stress and sediment transport calculations for swash zone modelling. Coast. Eng. 45, 53–67.

Nielsen, P., Callaghan, D.P., 2003. Shear stress and sediment transport calculations for sheet flow under waves. Coast. Eng. 47, 347–354.

Ribberink, J.S., Dohmen-Janssen, C.M., Hanes, D.M., McLean, S.R., Vincent, C., 2000. Near bed sand transport mechanisms under waves. Proc. 21st Int. Con./Coastal Eng., Sydney. ASCE, New York, pp. 3263–3276.

Sarpkaya, T., 1976. Vortex shedding and resistance in harmonic flow about smooth and rough circular cylinders at high Reynolds numbers. Rep. NPS-59SL76021. U.S. Naval Postgraduate School.

Sleath, J.F.A., 1994. Bedload transport in oscillatory flow. In: Belogey, Rajaona, Sleath (Eds.), Sediment Transport Mechanisms in Coastal Environments and Rivers, Proc Euromech, vol. 310. World Scientific.

Sleath, J.F.A., 1999. Conditions for plug formation in oscillatory flow. Cont. Shelf Res. 19, 1643–1664.

Svendsen, I.A., Jonsson, I.G., 1976. Hydrodynamics of Coastal Regions. Technical University of Denmark.

Terrile, E., 2004. The threshold of motion of coarse sediment particles by regular non-breaking waves. Master's Thesis, University of Genoa and Delft University of Technology (www.hydraulicengineering.tudelft.nl).

Tromp, M., 2004. The influence that fluid accelerations have on threshold of motion. Master's Thesis, Delft University of Technology (www.hydraulicengineering.tudelft.nl).

Zala-Flores, N., Sleath, J.F.A., 1998. Mobile layer in oscillatory sheet flow. J. Geophys. Res. 103 (C6), 12783–12793.